# Reviewer Comments to "Controls-Oriented Model for Secondary Effects of Wake Steering"

Jennifer King
National Renewable Energy Laboratory

December 10, 2020

The authors appreciate the feedback from the reviewers and believe that the manuscript has been much improved based on the reviewer comments. In particular, a reformulation of secondary steering and yaw-added recovery have been included that have proven to be more robust to varying wind farm configurations. Answers to the individual reviewer comments can be seen below.

Immediate improvements can be seen in the model in this figure:

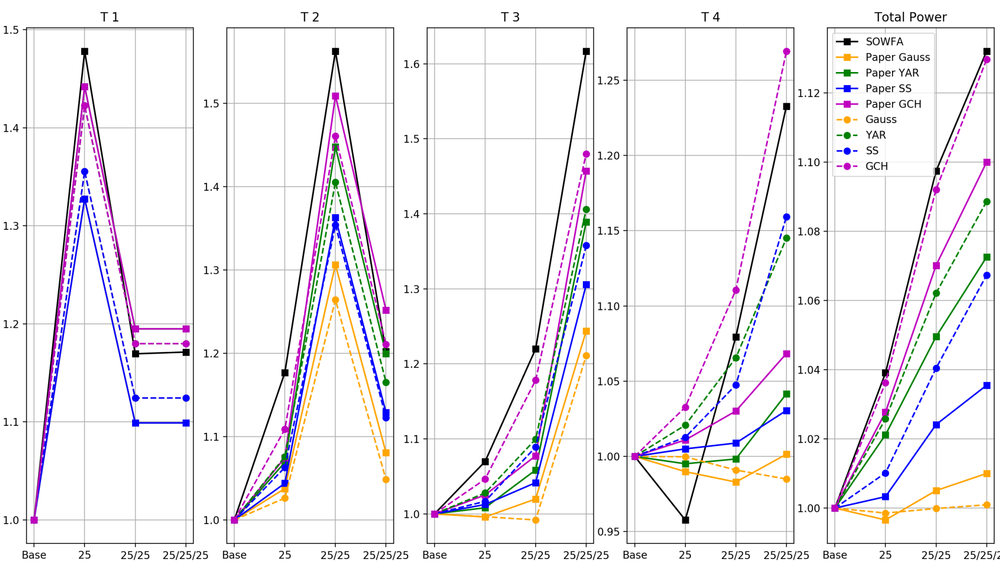


Figure 1: This figure shows the previous version of the model compared to the improvements made to the model based on reviewer suggestions.

# Reviewer 1

I read your article with great interest. You present a very important contribution to the literature, being a surrogate wind farm model that incorporates the effects of secondary steering. I find the translation of secondary steering to an "effective" yaw angle a very interesting, eloquent, and novel solution. This work will surely improve wind farm control algorithms and AEP predictions with such models. I envision that the proposed GCH model will replace the standard Bastankhah (Gaussian) wind farm model as the literature standard in the near future. My comments remain largely minor. That being said, I have a number of suggestions that may improve the clarity. and correctness of the article.

## Comments

- Generally, the manuscript needs to be proofread. Some sentences can be rephrased in a clearer manner and there is still a handful of spelling errors in the manuscript. Similarly, in figures, axis labels legends, captions, and subfigure titles need to be reconsidered and may. be made more clear. Note units and the size of text in figures compared to the regular manuscript font. Further, to simplify descriptions of simulation setups such as the first paragraph in Section 5, the authors could consider putting such information in a table instead.

  *The figures have been modified. In particular, figures 2, 3, 4, 7, and 14 have been added or modified to enhance the narrative of the manuscript.*

- Section 2 would greatly benefit from adding a figure that demonstrates the definition of various variables. Generally, I found it difficult to follow the derivations shown in this section. A figure or perhaps some restructuring of the text may benefit clarity. Also, please have a look at the consistency in definitions when moving from a single-wake model (Equation 1) to the wind farm model. In Equation 1, $y$ is defined as zero at the turbine while this is not necessarily the case in Equation 11, for example. Moreover, is it not true that $M_0 = C_T$?

  *The authors agree that a figure would be helpful to provide some useful context. Figure 1 has been added to address these issues. In addition, equation 1 has been updated and* $M_0$ *has been removed from the text everywhere..*

- Figure 1 shows the time-averaged flow fields from transient, turbulent SOWFA simulations. From what I am seeing here, and based on my own experience, I observe the following. The precursor simulation in SOWFA has a constant west inflow, I am assuming (270 degrees). This may cause certain faster regions of flow to "stack up" in the precursor simulation due to the cylcic boundary conditions. This explains why you have a higher inflow wind speed to the left and right side of your turbines (based on what I see in the plots of Figure 1). Now, since you are specifically looking at secondary steering effects, this may actually have an impact on your work. The ambient wind speeds are already higher to the left and right of the turbine due to the non-homogeneous mean inflow wind speeds in the precursor, and therefore also to the left and right of the downstream wake. This may induce more or less wake deflection than in a precursor without such "stack up" effects. I am not sure if you can address this in the current work, but you should consider this for future work.

*The authors agree with this assessment. The authors will be making the domains bigger in the future so that these streaks dissipate more and the authors can simulate cases at different spanwise locations to provide "bounds" on the simulations to make sure that these streaks are not exacerbating, or muffling, the effects of wake steering.*

- The GCH model is compared to the Gaussian model in Figure 4. It may be nice to (instead) show the wake outlines (centerline + $\sigma_y$, centerline - $\sigma_y$) of the two models in a single plot to more clearly show the additional deflection achieved with the GCH model. This would also show that the wake behind turbine 1 is identical between the two models.

  *The authors really appreciate this insight and have added these figures for the 3 turbine and the five turbine case that shows the influence of secondary steering from GCH. See figures 3, 4, and . A figure has been added to target the centerline. The boundaries of the wakes do not change significantly between models and were left off the figure to minimize clutter.*

- Figure 8 shows the power values measured from SOWFA. The default SOWFA implementation on Github has a bug where the generatorPower file in the turbineOutput folder is erroneously multiplied with a factor fluidDensity. This causes the power measurements to be a factor 1.225 too high in our own simulations, for which we have to correct manually. Have you considered this in your own work? It makes no difference in the other figures in which relative power productions are shown, but it does in Figure 8 where absolute values are shown.

  *Yes, this has been corrected in the version of SOWFA that is being used for this paper.*

- Sections 3-6 show a thorough analysis of the GCH and the Gaussian model, their differences, and how this reflects in simulation. This is very valuable. Though, due to the sheer amount of results, it can be a bit overwhelming. I wonder if the observations made in the 2- and 3-turbine analysis can also be made by only looking at the 5-turbine analysis.

  *The authors have removed the two turbine results and focused on three turbine, five turbine, and the wind farm results. The three turbine results were kept because of the sweep of yaw angles at the low turbulence intensity case is helpful in visualizing the asymmetry that is achieved with this model. See Figure 6.*

- What is the difference in computational cost between the GCH and Gaussian model? You can find a highlighted manuscript with more detailed comments in the attachment.

  *A speed test was conduced and GCH is 3.5x slower than the standard Gaussian model due to the computation of V and W. This has been noted in the text.*

# Reviewer 2

This manuscript presents an improved wake model, denoted as Gauss-Curl Hybrid (GCH) model, which is obtained by coupling the existing Gaussian wake model and the curl model. The main objective of the proposed wake model is to improve accuracy in predictions of wakes and turbine power capture in presence of yaw steering and more importantly, the secondary steering on downstream turbines induced by upstream yawed rotors. From field experiments, the secondary wake steering seems beneficial to enhance power capture for wind farms.

After a comprehensive introduction, the Gaussian model and the curl model are reviewed in Sect. 2. Subsequently, the GCH model is introduced by coupling the two previous models. In Sect 3, the first analysis consists of the case with two turbines. Sects. 4 and 5 show the results for a three and 5 turbine cases, respectively. Finally, a wind farm case is analyzed in Sect. 6.

## Major Comments

- How much of the physics is preserved through this model, such as mass conservation, momentum budgets? In other words, should this model be considered an analytical or empirical model?

  *It is noted in the text that mass conservation and momentum budgets are not obeyed in this paper. The reviewer is referred to* `https://arxiv.org/pdf/2011.00894.pdf` *to see the authors' ongoing work to attempt to preserve more physics in this model.*

- Sect. 4 (Figs. 3 and 4) - An initial comparison is done visually between the wake velocity fields obtained from SOWFA and the models. I recommend visualizing the error between the models and the reference SOWFA data. You can also provide some global parameters, such as mean absolute percentage error. 3.

  *The authors agree that figures 3 and 4 could be more descriptive. The authors have updated Figures 3 and 4 to include the differences between the Gaussian model and the GCH model in terms of wake centerline. While the flow field is important to match, these analytical models are focused on making sure the powers are computed accurately at each turbine.*

- Figs. 5, 6 - While for positive yaw angles, the GCH model performs very well, for negative angles besides the large error, even the trend is completely missed. You should comment, if I did not miss it, how this under-performance affects applications for control or wind farm design.

  *Based on another Reviewer's comments, the authors have taken out the two-turbine section, but have made a comment in the three turbine section about not always predicting the negative yaw angles correctly. Typical yaw controllers are mostly focused on positive yaw angle implementations; however, the authors note that this is an important phenomenon to understand and will be the subject of future research.*

## Minor Comments

- Equation 1 - cross-check it, I guess brackets are missing in the exponential.

  *This was fixed. See Equation 1*

- P3 L22, there is a typo at $\sigma_z$.

  *This has been fixed.*

- P8 L8 - "Published in literature"; add some references.

  *Since the first draft of this paper was written, a few of the parameters in the turbulence model have been slightly updated as the authors have acquired more large eddy simulation and field results. However, the values used in the velocity deficit and the velocity deflection model are the same as used in Bastankhah 2016 and Niayfar 2015 and is now indicated in the text.*

# Reviewer 3

In this paper, a new analytical model (GCH) which takes into account the yaw added wake recovery and the secondary wake steering effects is proposed to predict the wind farm power production under active yaw control. Overall, it is an interesting and promising piece of work. Nevertheless, the equations in this paper are in a mess. Some are wrong. Some are given without rigorous theoretical justification. These issues bother the reviewer a lot and have to be fixed prior to publication. Detailed comments are as follows:

## Major Comments

- Equations (11) - (18) are incorrect. Take equation (11) as an example. The induced spanwise velocity ($V$) should be related to the vertical distance to the vortex center ($z$-$z_h$), instead of the spanwise distance ($y$-$y_0$). The correct form is:

$$V_{\text{wake rotation}} = \frac{-\Gamma_{wr}(z - z_h)}{2\pi\left((y - y_0)^2 + (z - z_h)^2\right)}(\ldots)$$

  *The authors note the inconsistencies in the paper and have corrected these equations as the reviewer indicates.*

- Substituting equation (4) into Equation (3), we obtain $M_0 = C_T$. Why introduce two symbols to represent the thrust coefficient?

  *The authors have removed $M_0$ and $C_0$.*

- In Equation (6), the physical meaning of $u_0$ is the wake velocity at the onset of the far wake, instead of "the velocity behind the rotor" given by the authors.

  *This has been fixed.*

- Equation (9) is different from that in Bastankhah and Porte-Agel (2016). The authors changed the original term $1.6\sqrt{\frac{\sigma_y \sigma_z}{d^2 \cos\gamma}}$ to $1.6\sqrt{\frac{\sigma_y \sigma_z}{\sigma_{y0}\sigma_{z0}}}$. This doesn't hold, as $\sigma_{y0}\sigma_{z0} \neq d^2 \cos\gamma$. In fact, they differ approximately by a factor of 10.

  *The authors note the difference. However, the authors were referring to equation 5.8 from (Bastankhah 2016, see reference below). There are other differences between the two equations that must take care of this difference although the authors admit they have not worked through this by hand.*

  *Bastankhah, M. and Porté-Agel, F.: Experimental and theoretical study of wind turbine wakes in yawed conditions, Journal of Fluid Mechanics, 806, 506–541, 2016*

- In Section 2.3, the authors conjectured a new effect called "added wake recovery due to yaw misalignment" and stated "the wake recovers more when the turbine is operating in misaligned conditions..." In order to make such a statement, the authors should provide some quantitative evidences, or at least give a reference. Additionally, if this effect does exist, instead of using a complex equation (equation (23)), why not just increase the wake recovery rate, $k_y$?

  *After some rigorous testing, the authors agree that the current approach was not robust to all wind farm layouts. The authors have since improved this formulation as the reviewer suggests to more directly affect the recovery rate through an increase in TI as described in Section 2.3.*

- Equation (23) is given without rigorous theoretical derivation, which is unacceptable to the reviewer. What is the exact control volume used to apply momentum conservation? Why an artificial parameter, $\alpha_r$ is introduced? Detailed theoretical derivations should be given in the appendix.

  *The authors understand this confusion and have changed the formulation of the yaw added wake recovery from a control volume analysis to effectively increasing the turbulent mixing behind the rotor as indicated in Section 2.3.*

- In Section 2.3.1, instead of computing the effective yaw angle based on equation (24), why not directly use the ratio of total transverse velocity to freestream velocity to estimate $\gamma_{eff}$?

  *The authors have updated the way that the effective yaw angle is computed by directly using spanwise velocity. Although this might not be exactly what the reviewer had in mind, it provides a more robust solution than the previous iteration of the paper.*

- The figures in this paper are not well presented. Labels are hardly recognizable and the information in figures 2, 12, 13, and 14 can't be grasped at first sight.

  *The authors have done their best to address the readability of each of the figures as well as add a few figures to address the model setup and more clearly address the differences between the Gaussian and the GCH model.*

- Line 22 on page 3: $sigma_z$

  *This has been addressed.*

# Controls-Oriented Model for Secondary Effects of Wake Steering

Jennifer King[1], Paul Fleming[1], Ryan King[1], Luis A. Martínez-Tossas[1], Christopher J. Bay[1], Rafael Mudafort[1], and Eric Simley[1]

[1]National Wind Technology Center, National Renewable Energy Laboratory, Golden, CO, 80401, USA

*Correspondence to:* Jennifer King (jennifer.king@nrel.gov)

**Abstract.** This paper presents a model to incorporate the secondary effects of wake steering in large arrays of turbines. Previous models have focused on the aerodynamic interaction of wake steering between two turbines. The model proposed in this paper builds on these models to include yaw-induced wake recovery and secondary steering seen in large arrays of turbines when wake steering is performed. Turbines operating in ~~yaw-misaligned~~ yaw misaligned conditions generate counter-rotating vortices that entrain momentum and contribute to the deformation and deflection of the wake at downstream turbines. Rows of turbines can compound the effects of wake steering that benefit turbines far downstream. This model quantifies these effects and demonstrates that wake steering has greater potential to increase the performance of a wind farm ~~because of~~ due to these counter-rotating vortices ~~,~~ especially for large rows of turbines. This is validated using numerous ~~large-eddy simulations for two-turbine,~~ large eddy simulations for three-turbine, five-turbine, and ~~38-turbine~~ wind farm scenarios.

## 1 Introduction

Wake steering is a type of wind farm control in which wind turbines in a wind farm operate with an intentional yaw misalignment to mitigate the effects of its wake on downstream turbines in order to increase overall combined wind farm energy production (Wagenaar et al. (2012)). To design model-based controllers for wake steering, engineering models of the aerodynamic interactions between turbines are needed. Engineering models, in this context, are computationally efficient models that include enough physics to predict ~~wake-steering~~ wake steering behavior while running fast enough to be optimized in ~~real time~~real-time. These models can then be used in the design of wind farm control strategies (Simley et al. (2019); Fleming et al. (2019a)), layout optimizations (Gebraad et al. (2017); Stanley and Ning (2019)), or real-time control (Annoni et al. (2019)).

An early model of wake steering was provided in Jiménez et al. (2010). This model was combined with the Jensen model (Jensen (1984)) in the ~~multizone~~ multi-zone wake model in ~~FLOW Redirection and Induction in Steady State (FLORIS )~~ FLORIS (Gebraad et al. (2016)). The model was compared with large-eddy simulations (LES) using the Simulator ~~fOr~~ for Wind Farm Applications (SOWFA~~; Churchfield et al. (2014)) ,~~, Churchfield et al. (2014)) and several additional corrections including division of the wake into separate zones were added to better capture the aerodynamic interactions.

Several recent papers proposed a new ~~wake-deficit and wake-deflection~~ wake deficit and wake deflection model based on Gaussian self-similarity (Bastankhah and Porté-Agel (2014, 2016); Niayifar and Porté-Agel (2015); Abkar and Port-Agel (2015)). This model includes added turbulence ~~caused by~~ due to the turbine operation that influences wake recovery (Crespo et al. (1999)). In addition, this model has ~~minimal~~ some tuning parameters and includes atmospheric parameters that can be measured such as turbulence intensity (Niayifar and Porté-Agel (2015)). This model is commonly referred to as the Bastankah model, EPFL model, or Gaussian model. We will use the term Gaussian for the remainder of the paper. The Gaussian model was included as a wake model within the FLORIS tool (NREL (2019)). It has been used to design a controller for a field campaign ~~(Fleming et al. (2019a)), study wake-steering~~ in Fleming et al. (2019a), study wake steering robustness (Simley et al. (2019)), and has been validated with lidar measurements (Annoni et al. (2018)). The Gaussian model is also used in wind farm design optimization in Stanley and Ning (2019).

One of the main issues observed with the Gaussian model in FLORIS is that the model tends to ~~underpredict~~ under-predict gains in power downstream with respect to LES and field data. In addition, Fleming et al. (2016) and Schottler et al. (2016) show wake steering is asymmetrical~~(~~, i.e., clockwise and counter-clockwise yaw rotations do not produce equal benefits at the downstream turbine~~).~~. An empirical term had been explored to address this in Gebraad et al. (2016); however, it still does not fully capture the asymmetries present in the wake of yaw-misaligned turbines.

Fleming et al. (2018a) ~~investigate~~ investigates the importance of considering explicitly the counter-rotating vortices generated in wake steering (Medici and Alfredsson (2006); Howland et al. (2016); Vollmer et al. (2016)) to fully describe wake steering in engineering models. These vortices deflect and deform the wake at the downstream turbine. ~~Fleming et al. (2018a) also note~~ It is also noted in Fleming et al. (2018a) that these vortices persist farther downstream and impact turbines that are third, fourth, etc. in the row. This is known as secondary steering~~(SS)~~. It was proposed that modeling the counter-rotating vortices generated in wake steering could provide a means to model this process and ~~show~~ how wake steering will function when dealing with larger turbine arrays. Further, Ciri et al. (2018), has shown that modeling/accounting for the size of these vortices versus the ~~length scales~~ length-scales in the atmospheric boundary layer ~~explain variations in the~~ explains variations of performance of wake steering for differently sized rotors.

Martínez-Tossas et al. (2019) ~~provide~~ provides a wake model, known as the curl model, ~~that~~ which explicitly models these vortices. The paper shows that modeling the vortices can predict the deflection of the wake in misaligned conditions as well as the change in wake shape and cross-stream flows observed in Medici and Alfredsson (2006); Howland et al. (2016); Vollmer et al. (2016); Fleming et al. (2018a). However, the ~~Reynolds-averaged Navier-Stokes (RANS)-like~~ RANS-like implementation of the curl model~~and flow-marching simulation solution significantly increase~~, and finite-difference solution scheme significantly increases the computation complexity (around ~~1,000x~~1000x).

This paper presents a hybrid wake model~~that~~, which modifies the Gaussian model (Bastankhah and Porté-Agel (2014, 2016); Niayifar and Porté-Agel (2015)), with analytic approximations made of the curl model in (Martínez-Tossas et al. (2019)). This hybrid model will be referred to as the Gauss-Curl Hybrid, or GCH model. We propose it as a compromise ~~that~~ which maintains the many advantages of the Gaussian model, while incorporating corrections to address the following three important discrepancies:

1. Vortices drive a process of added yaw-based wake recovery, which increases the gain from wake steering to match LES and field results.

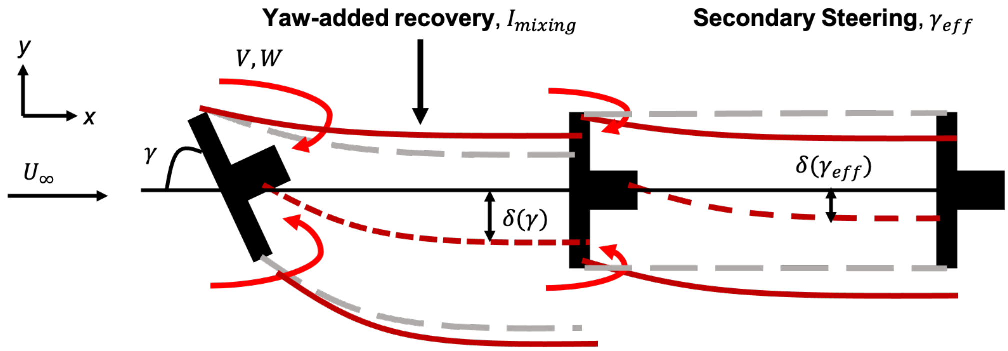


**Figure 1.** Model setup that includes yaw-induced effects such as yaw-added recovery and secondary steering. These effects manifest through the spanwise and vertical velocities that are generated from yaw-misaligned turbines. These effects are described in Section 2.2.

2. The interaction of the counter-rotating vortices with the atmospheric boundary layer ~~, shear layer ,~~ shear layer and wake rotation induces wake asymmetry naturally.

3. By modeling of the vortices, ~~SS,~~ secondary-steering and related multi-turbine effects are included, which will be important for evaluating wake steering for large wind farms.

In this paper, we will introduce the analytical modifications made to the Gaussian model in Section 2. We will use numerous LES simulations to show that the the improvements made in GCH ~~resolve~~ resolves the discrepancies identified above. This model will demonstrate how it compares with LES of ~~two-turbine~~ three turbines (Section ~~??), three-turbine (Section~~ 3), ~~and five-turbine wind arrays~~ five turbines (Section 4), and a 38-turbine wind farm (Section 5). In addition to these simulations, the proposed model is also validated using the results of a ~~wake-steering~~ wake steering field campaign at a commercial wind farm (Fleming et al. (2019b)).

## 2 Controls-Oriented Model

This section briefly ~~discusses~~ describes the Gaussian model used to describe the velocity deficit and the effects of wake steering in a wind farm. Figure 1 shows the setup for the controls-oriented model described in this paper. It is noted that mass and momentum are not conserved quantities in this model is the subject of ongoing research.

The proposed model, known as the Gauss-Curl Hybrid (GCH) model, builds upon the Gaussian model introduced in Bastankhah and Porté-Agel (2016); Abkar and Porté-Agel (2014); Abkar and Port-Agel (2015); Niayifar and Porté-Agel (2015) by including entrainment, asymmetry, and secondary ~~wake-steering~~ wake steering effects seen in LES ~~and~~ as well as field results.

### 2.1 Velocity Deficit Model

The wind turbine wake model used to characterize the velocity deficit behind a turbine in normal operation in a wind farm was introduced by several recent papers including Bastankhah and Porté-Agel (2016); Abkar and Port-Agel (2015); Niayifar and Porté-Agel (2015); Bastankhah and Porté-Agel (2014). The velocity deficit of the wake is computed by assuming a Gaussian wake, which is based on ~~the~~ self-similarity theory often used in free shear flows (Pope (2001)). An analytical expression for the ~~three-dimensional~~ streamwise velocity, $u_G$, behind a turbine is computed as:

$$\frac{u_G(x,y,z)}{U_\infty} = 1 - Ce^{\cancel{-(y-\delta)^2/2\sigma_y^2-(z-z_h)^2/2\sigma_z^2}-(y-y_0-\delta)^2/2\sigma_y^2 e^{-(z-z_h)^2/2\sigma_z^2}} \tag{1}$$

$$C = 1 - \cancel{\sqrt{1-\frac{(\sigma_{y0}\sigma_{z0})M_0}{\sigma_y\sigma_z}}}\sqrt{1-\frac{(\sigma_{y0}\sigma_{z0})C_T}{\sigma_y\sigma_z}} \tag{2}$$

$$\cancel{M_0 = C_0\left(2-C_0\right)}$$

$$\cancel{C_0 = 1-\sqrt{1-C_T}}$$

where $C$ is the velocity deficit at the wake center, $U_\infty$ is the freestream velocity, $\delta$ is the wake deflection (see Section 2.1.1), $y_0$ is the spanwise position of the turbine, $z_h$ is the hub height of the turbine, $\sigma_y$ defines the wake width in the $y$ direction, and ~~$sigma_z$~~ $\sigma_z$ defines the wake width in the $z$ direction. ~~Each of these parameters is defined with respect to each turbine.~~ The subscript “0” refers to the initial values at the start of the far wake, which is dependent on ambient turbulence intensity, $I_0$, and the thrust coefficient, $C_T$. For additional details on ~~near-wake~~ the onset of the far-wake calculations, the reader is referred to Bastankhah and Porté-Agel (2016). Abkar and Port-Agel (2015) demonstrate that ~~$\sigma_y$ and $\sigma_z$ grow~~ the wake expands at different rates based on lateral wake meandering (~~$y$~~ $\sigma_y$ direction) and vertical wake meandering (~~$z$~~ $\sigma_z$ direction). The velocity distributions ~~$\sigma_y$ and~~ $\sigma_z$ and $\sigma_y$ are defined as:

$$\frac{\sigma_z}{D} = k_z\frac{(x-x_0)}{D} + \frac{\sigma_{z0}}{D} \quad \text{where } \frac{\sigma_{z0}}{D} = \frac{1}{2}\sqrt{\frac{u_R}{U_\infty + u_0}} \tag{3}$$

$$\frac{\sigma_y}{D} = k_y\frac{(x-x_0)}{D} + \frac{\sigma_{y0}}{D} \quad \text{where } \frac{\sigma_{y0}}{D} = \frac{\sigma_{z0}}{D}\cos\gamma \tag{4}$$

where $D$ is the rotor diameter, $u_R$ is the velocity at the rotor, $u_0$ is the velocity at the start of the far wake, $k_y$ defines the wake expansion in the lateral direction, and $k_z$ defines the wake expansion in the vertical direction. For this study, $k_y$ ~~ad~~ and $k_z$ are set to be equal ~~,~~ and the wake expands at the same rate in the lateral and vertical directions. The wakes are combined using the traditional sum of squares method (Katić et al. (1986)), although alternate methods are proposed in Niayifar and Porté-Agel (2015).

This wake model also computes added turbulence generated by turbine operation and ambient turbulence conditions. For example, if a turbine is operating at a higher thrust, this will cause the wake to recover faster. Conversely, if a turbine is operating at a lower thrust, this will cause the wake to recover slower. Conventional linear flow models have a single wake expansion parameter that does not change under various turbine operating conditions. Niayifar and Porté-Agel (2015) provided a model that incorporated added turbulence due to turbine operation. Added turbulence is computed using (Crespo et al. (1999) ):

$$I^{+} = 0.5a^{0.8}I^{0.1}(x/D)^{-0.32} \tag{5}$$

where $I$ is the ambient turbulence intensity. The values used in this equation are slightly different from those in Niayifar and Porté-Agel (201 and have been tuned to large-eddy simulations.

#### 2.1.1 Wake Deflection

In addition to the velocity deficit, a ~~wake-deflection~~ wake deflection model is used to describe the ~~turbine behavior in~~ flow behavior behind a yaw-misaligned ~~conditions that occur~~ turbine, which occurs when performing wake steering and is also implemented based on Bastankhah and Porté-Agel (2016). The initial angle of wake deflection, $\theta$, ~~caused by~~ due to yaw misalignment is defined as:

$$\theta \approx \frac{0.3\gamma}{\cos\gamma}\left(1-\sqrt{1-C_T\cos\gamma}\right) \tag{6}$$

The initial wake deflection, $\delta_0$, is then defined as:

$$\delta_0 = x_0 \tan\theta \tag{7}$$

where $x_0$ indicates the length of the near wake~~, which is typically on the order of 3 rotor diameters~~. This can be computed analytically based on Bastankhah and Porté-Agel (2016).

The total deflection of the wake ~~caused by~~ due to yaw misalignment is defined as:

$$\delta = \delta_0 + \frac{\gamma E_0}{5.2}\cancel{\sqrt{\frac{\sigma_{y0}\sigma_{z0}}{k_y k_z M_0}}\ln\left[\frac{\left(1.6+\sqrt{M_0}\right)\left(1.6\sqrt{\frac{\sigma_y\sigma_z}{\sigma_{y0}\sigma_{z0}}}-\sqrt{M_0}\right)}{\left(1.6-\sqrt{M_0}\right)\left(1.6\sqrt{\frac{\sigma_y\sigma_z}{\sigma_{y0}\sigma_{z0}}}+\sqrt{M_0}\right)}\right]}\sqrt{\frac{\sigma_{y0}\sigma_{z0}}{k_y k_z C_T}}\ln\left[\frac{\left(1.6+\sqrt{C_T}\right)\left(1.6\sqrt{\frac{\sigma_y\sigma_z}{\sigma_{y0}\sigma_{z0}}}-\sqrt{C_T}\right)}{\left(1.6-\sqrt{C_T}\right)\left(1.6\sqrt{\frac{\sigma_y\sigma_z}{\sigma_{y0}\sigma_{z0}}}+\sqrt{C_T}\right)}\right] \tag{8}$$

where $E_0 = C_0^2 - 3e^{\frac{1}{12}}C_0 + 3e^{\frac{1}{3}}$. See Bastankhah and Porté-Agel (2016) for details on the derivation. The tuning parameters used in this paper are consistent with values from Bastankhah and Porté-Agel (2016) and Niayifar and Porté-Agel (2015).

### 2.2 Spanwise and Vertical Velocity Components

The spanwise and vertical velocity components are currently not computed in the Gaussian model, but they are ~~a critical component~~ critical components for modeling the effects of wake steering. These velocity components can be computed based on wake rotation and yaw misalignment ~~,~~ as shown in Martínez-Tossas et al. (2019) and Bay et al. (2019).

Wake rotation is included by modeling ~~the effects of rotation using~~ a Lamb-Oseen vortex~~to de-singularize the behavior~~ , which makes sure that the vortex is not a singular point near the center of the rotor. The circulation strength for the wake rotation vortex is now:

$$\Gamma_{\mathrm{wr}} = \frac{\pi(a-a^2)U_\infty D}{\lambda} \tag{9}$$

where $a$ is the axial induction factor of the turbine ~~,~~ and $\lambda$ is the tip-speed ratio~~.~~ , which is assumed to be a user-input, i.e. not computed within the FLORIS framework. See Martínez-Tossas et al. (2019) for additional details. Axial induction can be mapped to $C_T$ using (Bastankhah and Porté-Agel (2016)):

$$a = \frac{1}{2\cos\gamma}\left(1-\sqrt{1-C_T\cos\gamma}\right) \tag{10}$$

The vertical and spanwise velocities can then be computed using the strength of the vortex, $\Gamma$, by:

$$V_{\text{wake rotation}} = \frac{\Gamma_{\mathrm{wr}}(y-y_0)}{2\pi\left((y-y_0)^2+(z-z_h)^2\right)} \frac{\Gamma_{\mathrm{wr}}(z-z_h)}{2\pi\left((y-y_0)^2+(z-z_h)^2\right)}\left(1-e^{\frac{-((y-y_0)^2-(z-z_h))^2}{\epsilon^2}}\right) \tag{11}$$

$$W_{\text{wake rotation}} = \frac{\Gamma_{\mathrm{wr}}(z-z_h)}{2\pi\left((y-y_0)^2+(z-z_h)^2\right)} \frac{-\Gamma_{\mathrm{wr}}(y-y_0)}{2\pi\left((y-y_0)^2+(z-z_h)^2\right)}\left(1-e^{\frac{-((y-y_0)^2-(z-z_h))^2}{\epsilon^2}}\right) \tag{12}$$

where $y_0$ is the spanwise position of the turbine, ~~and~~ $\epsilon$ represents the size of the vortex core. In this paper, $\epsilon = 0.3D$, similar to Martínez-Tossas et al. (2019).

In addition to the wake rotation, when a turbine is operating in yaw-misaligned conditions, the turbine generates a collection of smaller counter-rotating vortices that is approximated as one pair of large counter-rotating vortices that are released at the top and the bottom of the rotor ~~. This is an approximation to the counter-rotating vortices defined in Martínez-Tossas et al. (2019) in that this model approximates the vortices as one at the top and bottom of the rotor, rather than a collection of smaller vortices. This is similar to what is done in Shapiro et al. (2018).~~ and generate additional spanwise and vertical velocity components that need to be accounted in this approach (Martínez-Tossas et al. (2019); Shapiro et al. (2018)). The strength of these vortices, $\Gamma$, can be computed as ~~$\Gamma$~~ and is a function of the yaw angle, $\gamma$~~:~~ , (Martínez-Tossas et al. (2019)):

$$\Gamma(\gamma) = \frac{\pi}{8}\rho D U_\infty C_T \sin\gamma\,(\cos\gamma)^2 \tag{13}$$

where $\rho$ is the air density.

As is done with wake rotation, The spanwise ~~$V$ and vertical $W$ velocity components can be~~ and vertical velocity components, $V$ and $W$, is computed based on the strength of the ~~wake rotation and~~ yaw misalignment of a turbine. The spanwise velocity can be computed as:

$$V_{\text{top}} = \frac{\Gamma(y-y_0)}{2\pi\left((y-y_0)^2+(z-(z_h+R))^2\right)} \frac{\Gamma(z-z_h+D/2)}{2\pi\left((y-y_0)^2+(z-(z_h+D/2))^2\right)}\left(1-e^{\frac{-((y-y_0)^2-(z-(z_h+R)))^2}{\epsilon^2}\frac{-((y-y_0)^2-(z-(z_h+D/2)))^2}{\epsilon^2}}\right)$$

(14)

$$V_{\text{bottom}} = \frac{\Gamma(y-y_0)}{2\pi\left((y-y_0)^2+(z-(z_h-R))^2\right)} \frac{\Gamma(z-z_h-D/2)}{2\pi\left((y-y_0)^2+(z-(z_h-D/2))^2\right)} \left(1-e^{\frac{-((y-y_0)^2-(z-(z_h-R)))^2}{\epsilon^2} \frac{-((y-y_0)^2-(z-(z_h-D/2)))^2}{\epsilon^2}}\right) \tag{15}$$

where ~~$R$ is the turbine radius, and~~ $V_{\text{top}}$ and $V_{\text{bottom}}$ are ~~the spanwise velocities generated~~ velocity deficit functions that originate from the rotating vortex at the top and bottom of the rotor, respectively. $\Gamma_{\text{top}}$ and $\Gamma_{\text{bottom}}$ are computed using the velocity at the top and bottom of the rotor based on the shear present at the rotor. In general, $\Gamma_{\text{top}}$ will be stronger than $\Gamma_{\text{bottom}}$.
The spanwise and vertical velocities are combined using a linear combination at downstream turbines ~~,~~ as is done in ~~Martínez-Tossas et al. (2~~ ~~and Bay et al. (2019)~~Martínez-Tossas et al. (2015); Bay et al. (2019). The total spanwise velocity is:

$$V_{\text{wake}} = V_{\text{top}} + V_{\text{bottom}} + V_{\text{wake rotation}} \tag{16}$$

Similarly, the vertical velocity can be written as:

$$W_{\text{top}} = \frac{\Gamma_{\text{top}}(z-(z_h+R))}{2\pi\left((y-y_0)^2+(z-(z_h+R))^2\right)} \frac{-\Gamma_{\text{top}}(y-y_0)}{2\pi\left((y-y_0)^2+(z-(z_h+D/2))^2\right)} \left(1-e^{\frac{-((y-y_0)^2-(z-(z_h+R)))^2}{\epsilon^2} \frac{-((y-y_0)^2-(z-(z_h+D/2)))^2}{\epsilon^2}}\right) \tag{17}$$

$$W_{\text{bottom}} = \frac{\Gamma_{\text{bottom}}(z-(z_h-R))}{2\pi\left((y-y_0)^2+(z-(z_h-R))^2\right)} \frac{-\Gamma_{\text{bottom}}(y-y_0)}{2\pi\left((y-y_0)^2+(z-(z_h-D/2))^2\right)} \left(1-e^{\frac{-((y-y_0)^2-(z-(z_h-R)))^2}{\epsilon^2} \frac{-((y-y_0)^2-(z-(z_h-D/2)))^2}{\epsilon^2}}\right) \tag{18}$$

The total vertical velocity can be computed as:

$$W_{\text{wake}} = W_{\text{top}} + W_{\text{bottom}} + W_{\text{wake rotation}} \tag{19}$$

~~Ground~~ Note, ground effects are included by adding mirrored vortices below the ground ~~,~~ as is done in Martínez-Tossas et al. (2019).

Finally, the vortices generated by the turbines decay as they move downstream. The dissipation of these vortices is described in Bay et al. (2019) and can be computed as:

$$V = V_{\text{wake}} \left( \frac{\epsilon^2}{4\nu_T \frac{(x-x_0)}{U_\infty} + \epsilon^2} \right) \tag{20}$$

$$W = W_{\text{wake}} \left( \frac{\epsilon^2}{4\nu_T \frac{(x-x_0)}{U_\infty} + \epsilon^2} \right) \tag{21}$$

where $\nu_T$ is the turbulent viscosity, which is defined using a mixing length model:

$$\nu_T = l_m^2 \left| \frac{\partial U}{\partial z} \right| \tag{22}$$

where $\cancel{l_m = \frac{\kappa z}{1+\kappa z/\lambda}}$ $l_m = \frac{\kappa z}{1+\kappa z/\lambda_T}$, $\kappa = 0.41$, and ~~$\lambda = D/8$. $\lambda$~~ $\lambda_T = D/8$. $\lambda_T$ is the value of the mixing length in the free atmosphere (~~Martínez-Tossas et al. (2019)~~Pope (2001)).

### 2.3 Added Wake Recovery ~~Caused By~~ due to Yaw Misalignment

The streamwise velocity and the wake deflection are influenced by ~~these velocity components~~the spanwise and vertical velocity components, $V$ and $W$. First, the wake recovers more when the turbine is operating in misaligned conditions ~~because of~~ due to the large-scale entrainment of flow into the wind farm domain. In this paper, we include ~~added wake recovery that is primarily caused by added entrainment from the presence of vertical velocity, $W$. Using a control volume approach for momentum conservation, the modified wake velocity, $u_r$, can be computed by adding an additional wake recovery component to the Gaussian model:~~ yaw-added recovery (YAR) as an added mixing term that influences the wake recovery $\sigma_y$ and $\sigma_z$ in the Gaussian model.

In Martínez-Tossas et al. (2019), it is assumed that the mean values of the spanwise and vertical velocities are small and we assume that the fluctuations in the spanwise and vertical directions are on the same order as the mean. The fluctuations induced by the counter-rotating vortices are defined in (20) and (21) above. The fluctuations influence the turbulent kinetic energy (TKE) that ultimately impacts the wake recovery. TKE, $k$, is defined as (Pope (2001)):

$$\cancel{u(x,y,z)}\, k_{\text{total}} = \frac{1}{2}\left( u_{\cancel{G}}'^2 + (\cancel{x,y,z}\, v' + v_{\text{curl}})^2 + \cancel{\text{added velocity from yaw}}\, (w' + w_{\text{curl}})^2 \right) \tag{23}$$

where ~~$u_G$ is computed by (1), $W$ is computed~~ $u'^2$ is determined from the ambient turbulence intensity defined, $v'^2$ is the average $V$ fluctuations at a turbine, assumed to be small, $v_{\text{curl}}$ is determined by (20), and $w'^2$ is the average $W$ fluctuations at a turbine, assumed to be small, and $w_{\text{curl}}$ determined by (21)~~(i. e.,~~.

In particular, $u'$ is determined by converting the ambient turbulence intensity into TKE by (Stull (2012)):

$$k = \frac{\left(\bar{U} * I\right)^2}{2/3} \tag{24}$$

where $\bar{U}$ is the average streamwise velocity at a turbine and $I$ is the ~~vertical velocity generated by wake rotation and the~~ turbulence intensity at a turbine. The streamwise fluctuations are then computed as:

$$u' = \sqrt{2k} \tag{25}$$

The TKE is converted to a turbulence intensity through the following (Stull (2012)):

$$I_{\text{total}} = \frac{\sqrt{\frac{2}{3} * k_{\text{total}}}}{U_i} \tag{26}$$

where $U_i$ is the average velocity at turbine $i$. The amount of turbulence generated from the counter-rotating ~~vortices present when a turbine is operating in misaligned conditions), and $\alpha_r$ is a tuning parameter that dictates how much the entrainment affects the wake recovery. For this paper, that term is set to $\alpha_r = 0.03$. The larger $\alpha_r$ is , the smaller the effect of entrainment is on the streamwise velocity component~~vortices can be calculated by:

$$I_{\text{mixing}} = I_{\text{total}} - I \tag{27}$$

where $I$ is the ambient turbulence.

### 2.3.1 ~~Secondary Steering Through~~ Incorporating secondary steering effects by the introduction of an Effective Yaw angle

In addition to added wake recovery, the model proposed in this paper is able to predict ~~SS. The wake-deflection~~ secondary steering that matches large-eddy simulations. The wake deflection model described in Section 2.1.1 can be used to describe the deflection of the wake for a ~~two-turbine~~ two turbine case. However, additional information is needed to describe the impact of yaw misalignment on turbines in large wind farms ~~,~~ as is shown in Fleming et al. (2018a).

Specifically, the vortices described in the previous section propagate far downstream, dissipate, and affect all turbines directly downstream of the turbine that generated the vortices. When they reach a downstream turbine, they impact the wake of the downstream turbine in a phenomenon called ~~SS~~ secondary steering (Fleming et al. (2018b)). The spanwise and vertical velocities generated by the counter-rotating vortices act like an effective yaw angle at the next turbine. In other words, the spanwise and vertical ~~velocities~~ velocity components of upstream turbines affect the deformation and deflection of a wake downstream as if the downstream turbine were implementing wake steering even when it is aligned with the flow. ~~This can be~~ In this model, these effects are approximated as an ~~apparent or~~ effective yaw angle. To model ~~SS~~secondary steering, an effective yaw angle is computed to describe the effect of the vortices generated at the upstream turbine on the downstream turbine wake. The effective yaw angle is computed using the mean spanwise velocity, $V$, present at the turbine rotor. The ~~presence of spanwise and vertical velocities generate an effective circulation that is responsible for deflecting and deforming the wake. At a downstream turbine, the strength of the effective circulation,~~ effective yaw angle, $\gamma_{\text{eff}}$, is ~~calculated by taking the inverse of (20)~~computed by finding the yaw angle that reproduces the approximate that spanwise velocity:

$$\cancel{\Gamma} V_{\text{eff}} = \cancel{\frac{1}{N}\sum_i^N \frac{2\pi V_i\left((y_i-y_0)^2+(z_i-z_h)^2\right)}{(y_i-y_0)\left(1-e^{\frac{-((y_i-y_0)^2-(z_i-z_h))^2}{\epsilon^2}}\right)}} V_{\text{wake}}(\gamma) \tag{28}$$

where ~~$V$ are the spanwise velocities inside the rotor area, and $N$ is~~ $\gamma$ is an array of yaw angles between $-45°$ and $+45°$. This determines what the yaw angle of the ~~number of points in the rotor area~~turbine would have needed to be to produce that same spanwise velocity. The effective yaw angle, $\gamma_{\text{eff}}$, is ~~then computed using $\Gamma_{\text{eff}}$ and solving for $\gamma$ in (13).~~ found by minimizing the difference between the effective spanwise velocity and the spanwise velocity calculated at the rotor:

$$\gamma_{\text{eff}} = \text{argmin}|\bar{V} - V_{\text{eff}}| \tag{29}$$

The total wake deflection can be computed using (8) where the total yaw angle, $\gamma$ ~~,~~is:

$$\gamma = \gamma_{\text{turb}} + \gamma_{\text{eff}} \tag{30}$$

where $\gamma_{\text{turb}}$ is the amount of yaw offset the turbine is actually applying. This $\gamma$ is used in (8) to compute the lateral deflection of the wake.

~~Because of~~ Due to the presence of the effective yaw angle, downstream turbines generally do not have to yaw as much as upstream turbines to produce large gains. This phenomenon was observed in a wind tunnel study (Bastankhah and Porté-Agel (2019)).

## 3 ~~Two-Turbine Analysis~~

~~In this section, SOWFA simulations were run for a variety of two-turbine scenarios. Each two-turbine scenario is run using both the Gaussian and the GCH model. The effects of SS will have no effect on two-turbine scenarios; thus, GCH is equivalent to only the~~ The addition of yaw-added recovery ~~(YAR) effect addressed in Section 2.3. Therefore, we will refer to the model as YAR in this section. This analysis focuses on a wind speed of 8 m/s with turbulence intensities of 6% and 10%, where spacing between the turbines is fixed at 7 rotor diameters, i.e., 7D. The Gaussian model and~~ and secondary steering effects has increased the computational time by 3.5×, e.g. a five turbine case takes 0.007s to run the GCH model ~~share the same tuning parameters and have been tuned to the same value, which is consistent with what has previously been published in literature. Only turbulence intensity (TI) and freestream velocity are changed between simulations to match LES. Mean wind speeds vary slightly between low- and high-turbulence scenarios (e.g.,~~ ~~$U_\infty = 8.34$ m/s for low-turbulence and $U_\infty = 8.38$ m/s for high-turbulence cases).~~ compared to 0.002s for the Gaussian model. However, the results in this paper indicate that when evaluating wake steering, GCH is necessary to include as the Gaussian model is not able to capture the compounding effects of wake steering.

~~The first turbine is fixed at one location, while its yaw angle is varied through a range of positive (counter-clockwise, CCW) and negative (clockwise, CW) yaw offsets. The second turbine is always aligned with the flow but is offset laterally -R,0,+R from the upstream turbine. The SOWFA simulations with the front turbines yawed +20 are illustrated in Fig. **??** (right column). Fig. **??** also shows cases with no yaw (middle column) and with -20° offset (left column). Simulations with +R offset are in the top row, 0R offset are in the middle row, and -R offset are in the bottom row.~~

~~Flow fields of streamwise velocity components for when the second turbine is offset +R (top), 0R or aligned (middle), and -R (bottom). The front turbine is yawed −20° (left column), 0° (middle column), and +20° (right column).~~

~~The results are analyzed by considering the percentage gain (or loss) in power of the second turbine from yawing the front turbine in each case either +20° (CCW) or -20° (CW). These results are shown in Fig. **??**. Most of the improvements in GCH~~

~~are expected to benefit larger arrays of turbine scenarios where SS plays a role. However, the suggested improvements in YAR can be seen in the asymmetry introduced by wake rotation and shear. This can be seen most clearly in the aligned 0R cases (middle row of Fig. ??). The initial Gaussian model assumes the gain on the second turbine is equivalent whether yawing positively or negatively, whereas YAR matches the pattern from SOWFA where the positive gains exceed the negative.~~

~~Results for percent change of power in the second turbine in each offset location, for each model, at 8 m/s and 6% turbulence intensity (left) and 10% turbulence intensity (right). The results are shown where the second turbine is offset +R (top row), 0R (middle row), and -R (bottom row).~~

~~The second improvement focuses on the magnitude of gains from positive yawing. For the four cases shown in Fig. ??, in which positive yawing is beneficial according to SOWFA, the Gaussian model significantly underestimates the gain in all cases. Further, considering the case in which positive yaw is harmful, -R, the Gaussian consistently overestimates the loss, while the YAR model more closely matches SOWFA by producing fewer negative results. However, YAR does not perform as well as the Gaussian model when predicting the gains of negative yaw when the second turbine is offset by -R. This will be subject to future research. A loads study of wake steering suggested that positive yaw angles are less harmful to turbines, and thus, mainly positive angles are used for wake steering (Damiani et al. (2017)).~~

## 3 Three-Turbine Analysis

~~Next~~First, the Gaussian model, GCH model, and SOWFA are compared in three-turbine array simulations. The three-turbine array demonstrates the benefits of ~~YAR effects~~ yaw-added recovery (YAR) effect as well as ~~SS~~secondary steering (SS). The following plots show the contributions of YAR and SS compared with the Gaussian model and the full GCH model, which ~~contain~~ contains both YAR and SS. The YAR and SS models are computed by disabling the model produced in Section 2.3 ~~and Section 2.3.1, respectively,~~ within the GCH model to isolate the two effects.

The ~~three-turbine~~ three turbine scenario was simulated at 8 m/s with 6% and 10% turbulence intensities and spaced $7D$ apart in the streamwise direction. Fig. 2 shows the flow fields from the SOWFA simulations for baseline (top row), the first turbine yawed 20° (middle row), and the first turbine yawed 20° and the second turbine yawed 10° (bottom row). For visual comparison, Fig. ~~?? shows the Gaussian model (left) and the GCH model (right)~~ 3 and Fig. 4 shows FLORIS computed using the GCH model where the first turbine is yawed 20° (~~top row~~Fig. 3) and the first turbine is yawed 20° and the second turbine is yawed 10° (~~bottom row). Visually, the impact of SS~~ Fig. 4). The impact of secondary steering is shown in the wake centerlines where the Gaussian model centerline is shown in blue and the wake centerline computed with GCH is shown in red. It can be seen ~~on the wake of the third turbine in the GCH model(right column)~~that there is steering on downstream turbines that are not yawed in the GCH model and there is no movement in the wake centerline in non-yawed turbines in the Gaussian model.

Next, several simulations were run at each turbulence intensity where the first turbine was yawed 20° ~~,~~ and the second turbine was yawed between -20° and +20°. ~~Figures~~Figure 5 and 6 ~~show~~ shows the relative power gains of the SOWFA simulations for turbulence intensities of 6% and 10% ~~, respectively ,~~ respectively relative to a baseline case of all turbines aligned. The SOWFA simulations are compared with the Gaussian model, YAR, SS, and the GCH model. The ~~turbines in the three-turbine~~

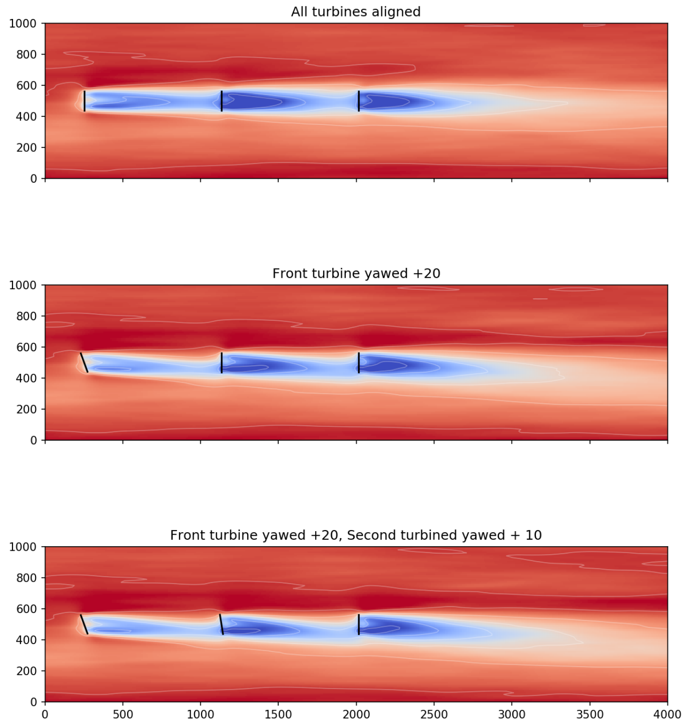


**Figure 2.** Three-turbine array in SOWFA where all turbines are aligned (top), the first turbine is yawed +20° (middle), and the first turbine is yawed +20° ~~,~~ and the second turbine is yawed +10°.

~~cases are labeled as Turbine 1 (most upstream turbine), Turbine 2 (middle turbine), and Turbine 3 (most downstream). The~~ power gains of Turbine 2 are shown in the left plot in Figs. 5 and 6, Turbine 3 is shown in the middle plot, and the total power gains are shown in the right plot.

The Gaussian model is not able to capture the secondary effects of wake recovery and ~~SS~~secondary steering. The Gaussian model is able to capture gains in ~~low-turbulence~~ low turbulence (6%) conditions~~(~~, see Fig. 5~~)~~. However, it does not see any gains when turbulence intensity is higher ~~, as shown in~~ as shown Fig. 6. ~~For~~ It is also important to note that for Turbine 3 and the total gains, the Gaussian model forecasts a change in power ~~that~~ which is symmetrical about changes in Turbine 2, whereas SS and the GCH model predict that a -10° yaw on a turbine, which is behind a turbine yawed +20° ~~,~~ is counter-productive, while a complementary +10° yaw is more valuable ~~then~~ than either Gauss or YAR would predict. The figures also show how the two

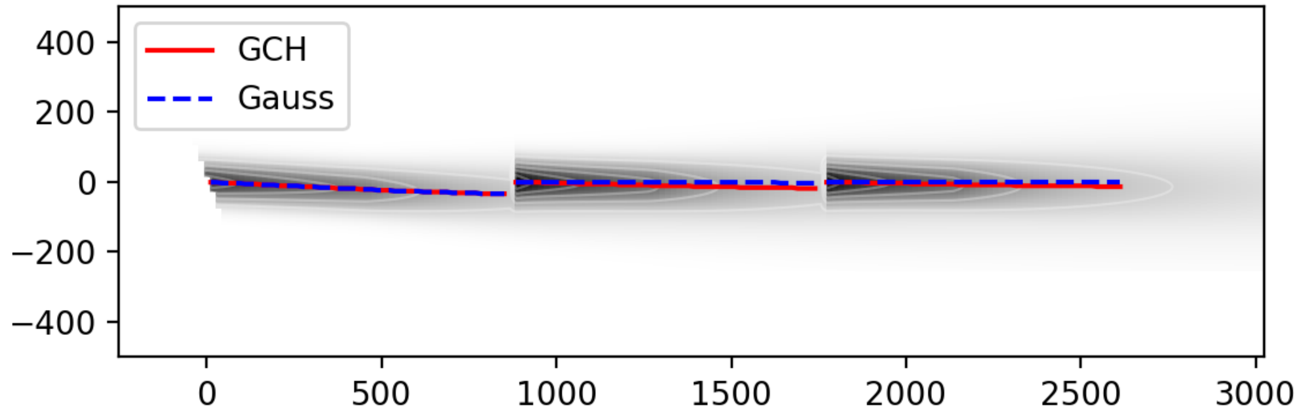


**Figure 3.** FLORIS results for the three-turbine case shown for the ~~Gaussian~~ the GCH model with the centerline of the wake computed for GCH (~~left~~red) and the ~~GCH~~ Gaussian model (~~right~~blue), where the first turbine is yawed 20°~~(top row), and the first turbine is yawed 20°, and the second turbine is yawed 10° (bottom row)~~.

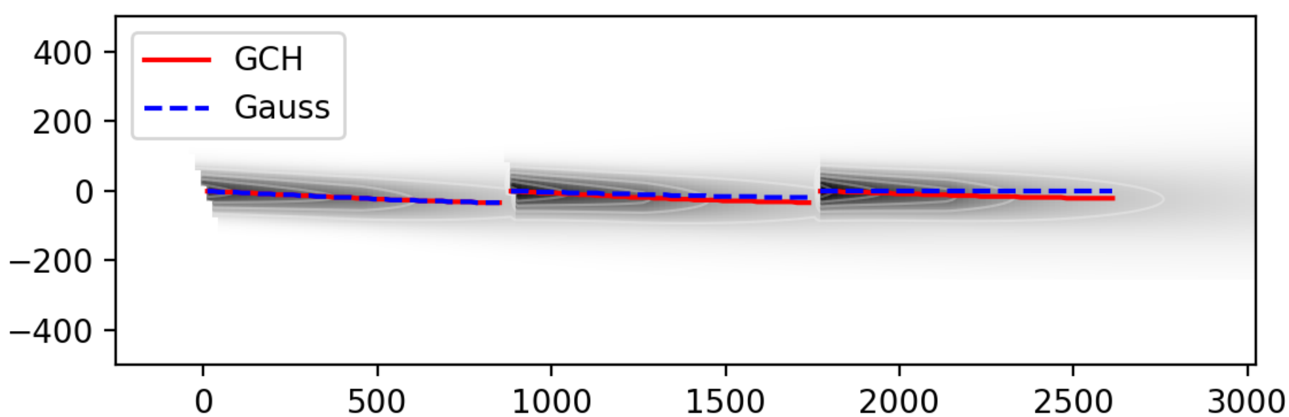


**Figure 4.** FLORIS results for the three-turbine case shown for the the GCH model with the centerline of the wake computed for GCH (red) and the Gaussian model (blue), where the first turbine is yawed 20° and the second turbine is yawed 10°.

added effects, YAR and SS, complement each other. YAR improves the prediction of the ~~second turbine (~~middle Turbine 2~~)~~, while SS can only improve the predictions farther downstream. The combined GCH model is most like LES in both ~~low- and high-turbulence scenarios.~~ low and high turbulence scenarios. It is important to note that GCH is able to capture the asymmetry of wake steering where the Gaussian model presents a symmetric solution. The GCH model matches better for positive yaw angles as this is the most common implementation in the field. However, future research will be done to improve the accuracy of wake steering for negative yaw angles.

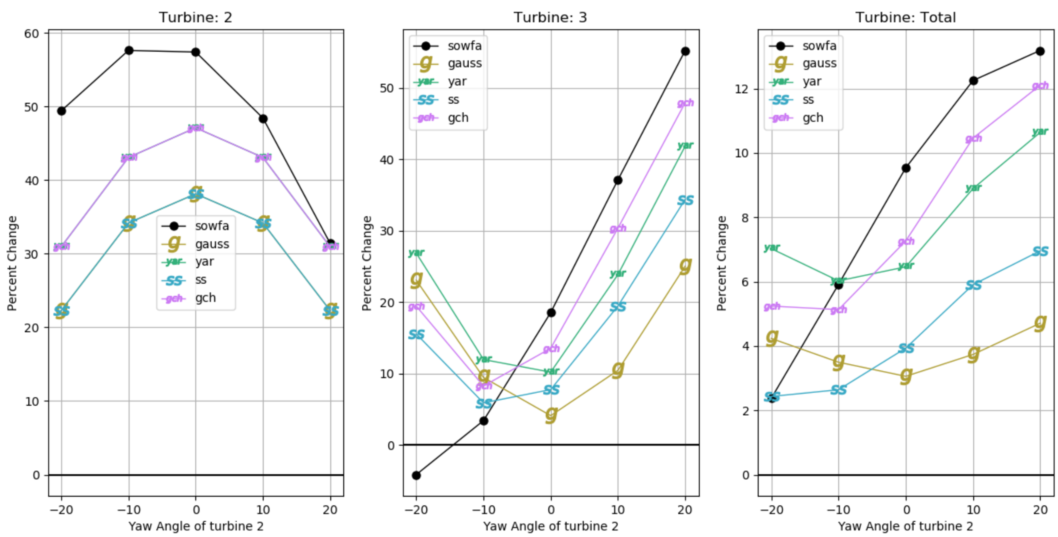


**Figure 5.** Comparison of changes in power when sweeping the angle of the second turbine~~(~~, i.e. ~~,~~Turbine 2~~)~~, when the angle of the first turbine~~(~~, i.e., Turbine 1 ~~)~~ is set to +20° where the wind speed was 8 m/s and the turbulence intensity was 6%. The results of the change in power of the third turbine, as well as the overall total of all three turbines, reflect the importance that the two yaw offsets are in the same direction.

## 4 Five-Turbine Analysis

Next, five turbines were simulated in SOWFA, the Gaussian model, and the GCH model for different combinations of yaw angles, starting with all aligned, the first turbine yawed 25°, the first and second turbine yawed 25°, and the first three turbines yawed 25°. Fig. 7 shows the flow field for GCH ~~in baseline conditions (top) and optimized conditions (bottom). The five-turbine~~ yawed conditions with the wake centerlines defined in blue for the Gaussian model and in red for the GCH model. It can be seen that the wake centerlines move more as there are more turbines in a line. The five turbine array was simulated with a wind speed of 8 m/s and turbulence intensities of 6% (labeled as low turbulence) and 10% (labeled as high turbulence). The turbines are spaced $6D$ in the streamwise direction.

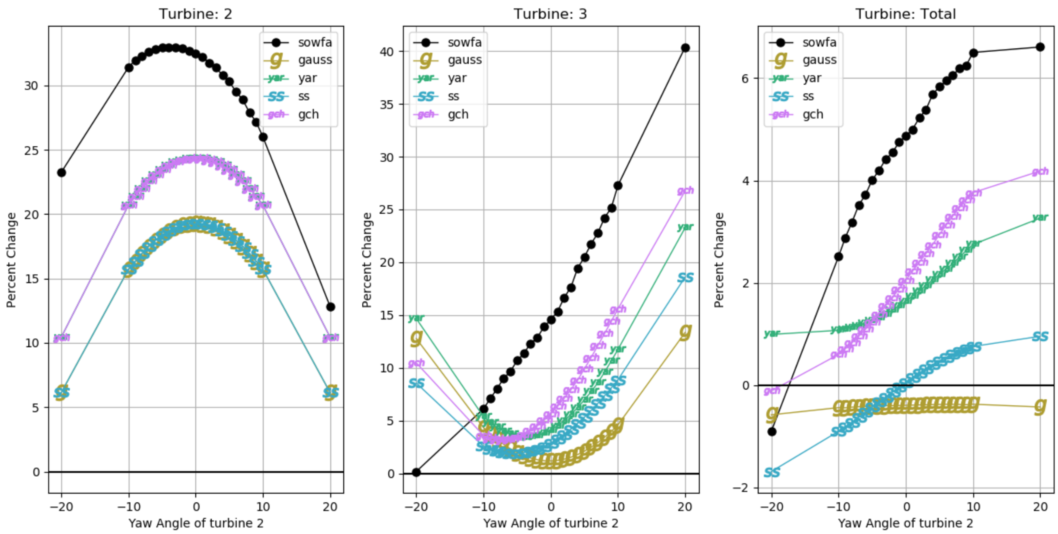


**Figure 6.** Comparison of changes in power when sweeping the angle of the second turbine~~(~~, i.e. ~~,~~ Turbine 2~~)~~, when the angle of the first turbine~~(~~, i.e., Turbine 1 ~~)~~ is set to +20° where the wind speed was 8 m/s and the turbulence intensity was 10%.

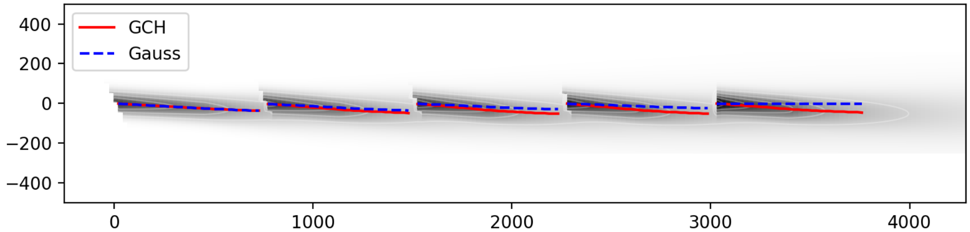


**Figure 7.** Flow field of ~~five~~ 5 turbines using GCH. The resulting centerline behind each turbine is shown for ~~the baseline case (top)~~ GCH in red and the ~~optimized case (bottom)~~Gaussian model in blue. The optimized yaw angles are based on the values shown in Table 1.

Fig. 8 shows the absolute powers of each turbine in the ~~five-turbine~~ five turbine array, excluding the first turbine, for ~~low-turbulence~~ low turbulence conditions. The GCH model is able to most closely capture the trends seen in SOWFA ~~,~~ especially when evaluating total turbine power. The power gains for each turbine are shown in Fig. 9. The Gaussian model is pessimistic about the potential gains for the ~~five-turbine~~ five turbine case. YAR and SS both contribute significantly to the total gains seen in the ~~five-turbine case. All~~ five turbine case. It should be noted that all models have a difficult time predicting the absolute power and the power gain of the last turbine. This may be resolved with a more rigorous “turbulence” model than the one used in this model~~(see Annoni et al. (2018))~~, see Annoni et al. (2018). In addition, this model does not directly account for ~~deep-array effects ,~~ deep array effects and this may also be a source of error and is a subject of ongoing research.

Fig. 10 shows the same ~~five-turbine~~ five turbine analysis for the ~~high-turbulence~~ high turbulence scenario (10% turbulence intensity). Again, the GCH model most closely follows the trends seen in SOWFA. The most notable difference between GCH and the Gaussian model is that the Gaussian model is extremely pessimistic about wake steering in high turbulence~~(i. e., there are no gains to be realized under these conditions).~~ . However, according to SOWFA, large gains are still expected from wake steering even in high turbulence. The GCH model is able to capture the power gains seen in SOWFA at ~~high-turbulence intensities ,~~ high turbulence intensities although GCH is still slightly ~~underpredicting~~ under-predicting the potential gains of wake steering.

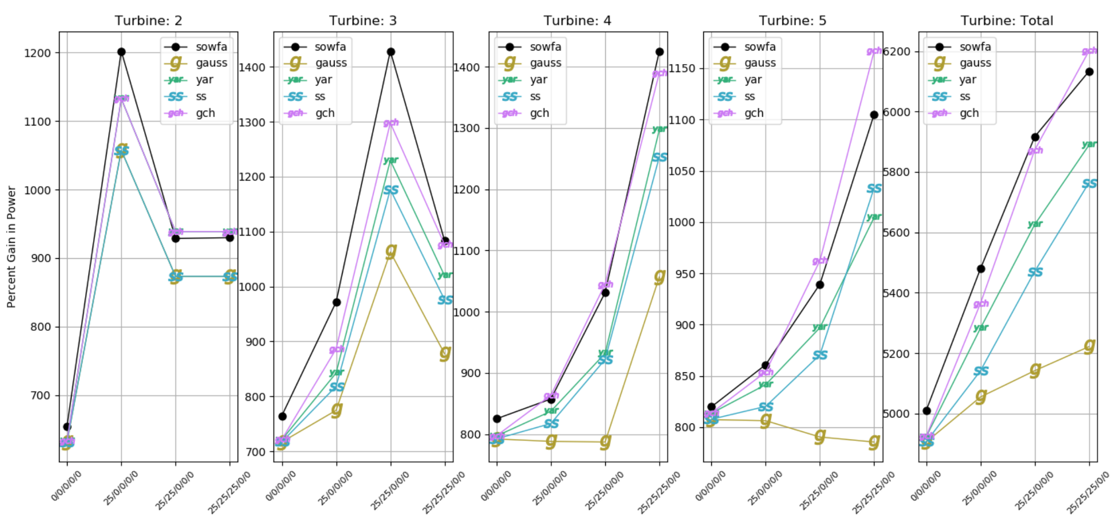


**Figure 8.** Absolute power values for each turbine (excluding the upstream turbine ~~0~~1) in the ~~five-turbine~~ five turbine array for a wind speed of 8 m/s and low turbulence~~(~~, i.e., 6% turbulence intensity~~)~~. Total turbine power is shown in the ~~far-right~~ far right plot. The $x$-axis shows the combination of yaw angles plotted.

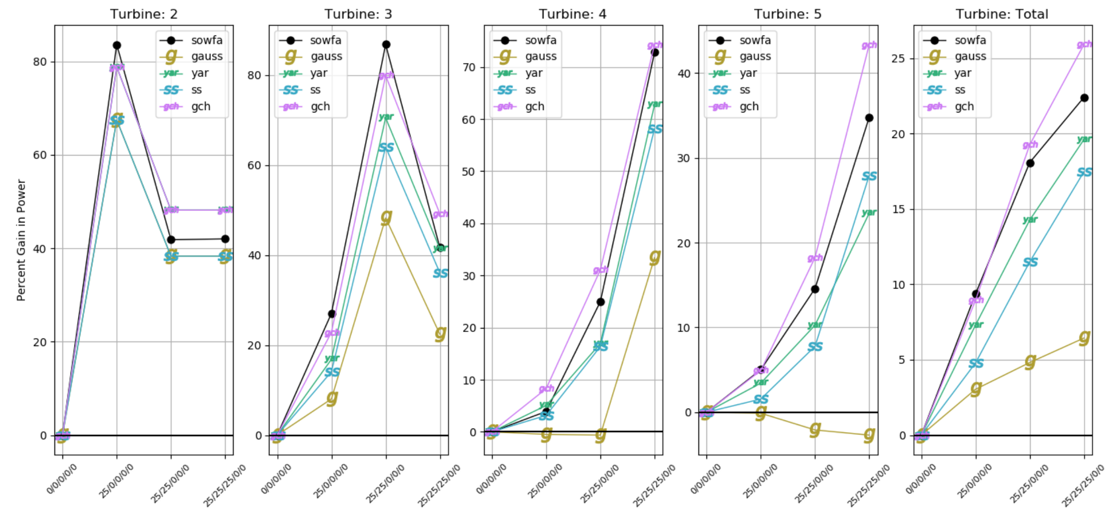


**Figure 9.** Power gains for each turbine (excluding the upstream turbine~~0~~) in the ~~five-turbine~~ five turbine array for a wind speed of 8 m/s and low turbulence~~(~~, i.e., 6% turbulence intensity~~)~~. Total power gain is shown in the ~~far-right~~ far right plot. The $x$-axis shows the combination of yaw angles plotted.

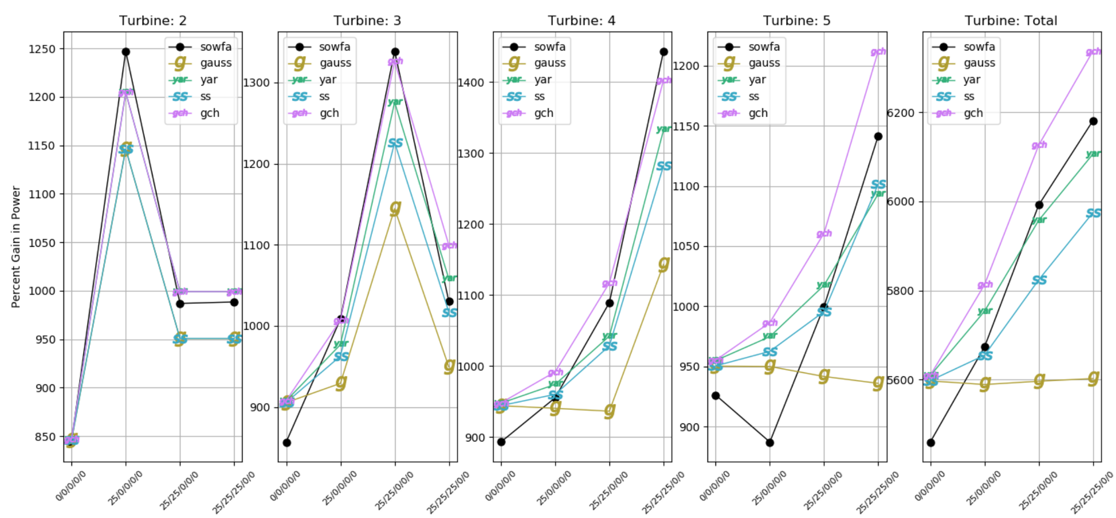


**Figure 10.** Absolute power values for each turbine (excluding the upstream turbine) in the ~~five-turbine~~ five turbine array for a wind speed of 8 m/s and high turbulence~~(~~, i.e., 10% turbulence intensity~~)~~. Total turbine power is shown in the ~~far-right~~ far right plot. The $x$-axis shows the combination of yaw angles plotted.

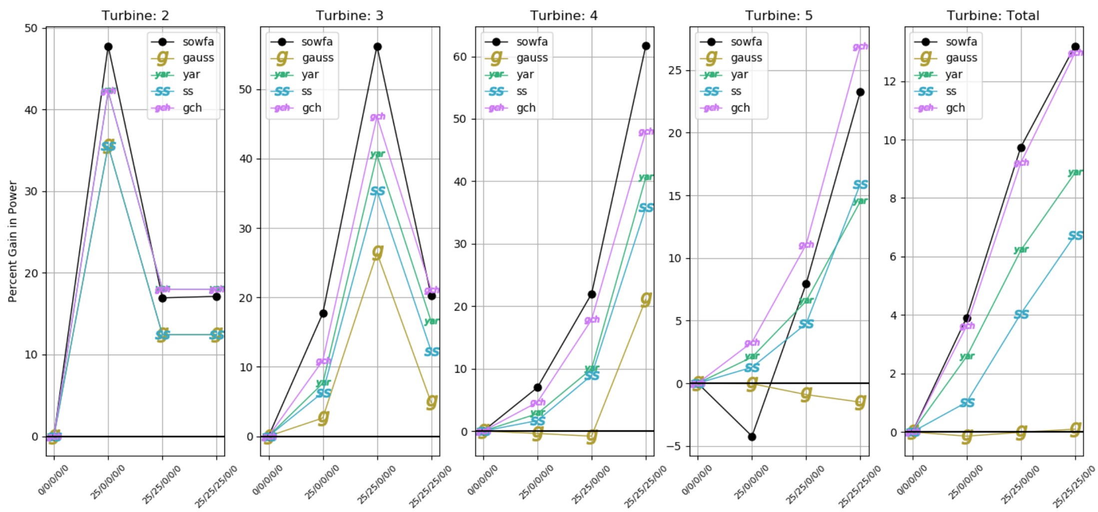


**Figure 11.** Power gains for each turbine (excluding the upstream turbine) in the ~~five-turbine~~ five turbine array for a wind speed of 8 m/s and high turbulence~~(~~, i.e., 10% turbulence intensity~~)~~. Total power gain is shown in the ~~far-right~~ far right plot. The $x$-axis shows the combination of yaw angles plotted.

### 4.1 Optimization of ~~Five-Turbine~~ Five Turbine Array

Engineering wake models in FLORIS are often used to determine optimal setpoints for wake steering and assess the performance of these setpoints. The results of optimizing the Gaussian and GCH models are compared in this section. Specifically, the Gaussian and GCH models were optimized individually for the ~~five-turbine case under low- and high-turbulence~~ five turbine case under low and high turbulence conditions. These yaw angles from each optimization were simulated in SOWFA. The power predicted in SOWFA, the Gaussian model, and the GCH model, for each set of yaw angles, are compared in Table 1. The results are compared to ~~:~~ 1) a baseline where the yaw angles of all turbines in the ~~five-turbine~~ five turbine array are zero, and 2) a naive strategy of simply maximizing yaw offsets, subject to an upper bound of 25° to limit structural loads, for all turbines except the last.

In both ~~low- and high-turbulence~~ low and high turbulence cases, the ~~GCH-optimized~~ GCH optimized yaw angles produced higher power gains in SOWFA compared with the Gaussian model, and also outperformed simply operating all turbines (except the last turbine) at a maximum yaw angle of 25°. ~~Similar~~ Similarly to results observed in a wind tunnel study in Bastankhah and Porté-Agel (2019), GCH produces decreasing yaw angles at farther downstream turbines ~~,~~ indicating that GCH is taking advantage of the effective yaw angle produced by the counter-rotating vortices generated by upstream turbines. Note that GCH more closely predicts the gain observed in SOWFA versus the Gaussian in all cases.

| Case | Turbine 1 | Turbine 2 | Turbine 3 | Turbine 4 | SOWFA Gain | Gauss Gain | GCH Gain |
|---|---|---|---|---|---|---|---|
| Low Turbulence | | | | | | | |
| ~~Gauss-optimized~~ Gauss optimized angles | 24.0° | 25.0° | 25.0° | 25.0° | 22.7% | ~~8.6~~7.9% | ~~21.9~~26.2% |
| ~~GCH-optimized~~ GCH optimized angles | 25.0° | 25.0° | 22.1° | 18.7° | **23.7%** | ~~8.3~~7.4% | ~~22.3~~27.7% |
| Max yaw angles | 25.0° | 25.0° | 25.0° | 25.0° | 22.9% | ~~8.5~~8.0% | ~~22.0~~26.4% |
| High Turbulence | | | | | | | |
| ~~Gauss-optimized~~ Gauss optimized angles | 12.9° | 23.4° | 19.7° | 14.1° | 7.5% | ~~0.5~~1.0% | ~~9.8~~12.4% |
| ~~GCH-optimized~~ GCH optimized angles | 24.2° | 24.4° | 22.7° | 16.5° | **14.3%** | ~~-0.2~~0.5% | ~~10.0~~14.0% |
| Max yaw angles | 25.0° | 25.0° | 25.0° | 25.0° | 13.1% | ~~-1.6~~0.2% | ~~9.1~~12.7% |

**Table 1.** ~~Five-turbine~~ Five turbine results for ~~low-~~ low and ~~high-turbulence~~ high turbulence conditions using SOWFA, the Gaussian model, and the GCH model.

## 5 Wind Farm Analysis

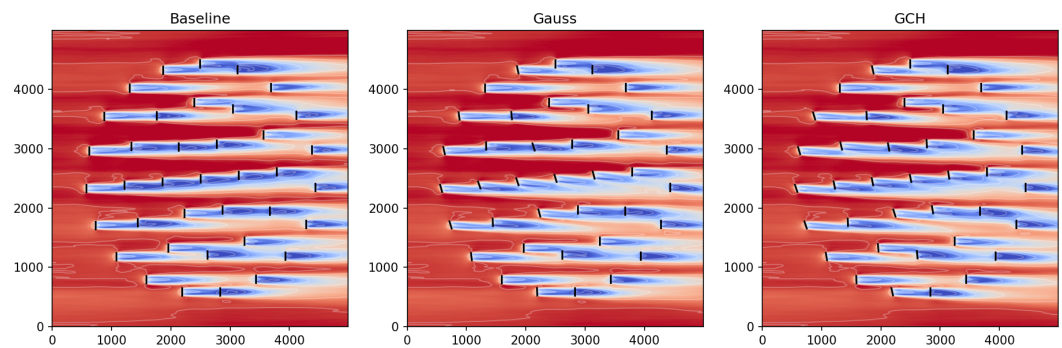


**Figure 12.** Flow field results from SOWFA where the wind direction is 270° (Case 2). The left plot shows the baseline case with all turbines aligned with the flow~~, the~~. The middle plot shows the flow field with yaw angles from the optimized Gaussian model ~~,~~ and the right plot shows the flow field with the yaw angles from the optimized GCH model.

Finally, a full wind farm analysis was performed to quantify the potential of wake steering when effects such as yaw-added recovery and ~~SS~~ secondary steering are included. For this analysis, we used a 38-turbine wind farm ~~, as used~~ used as in Thomas et al. (2019). The flow field for the baseline case is shown on the left in Fig. 12 where the wind direction is 270° ~~. The left plot shows the baseline case with all turbines~~ and all turbines are aligned with the flow. The middle plot shows the flow field with yaw angles from the optimized Gaussian model ~~,~~ and the right plot shows the flow field with the yaw angles from the optimized GCH model. The analysis was performed for two wind directions, 95° and 270°, and will be referred to as Case 1 and Case 2 ~~,~~ respectively.

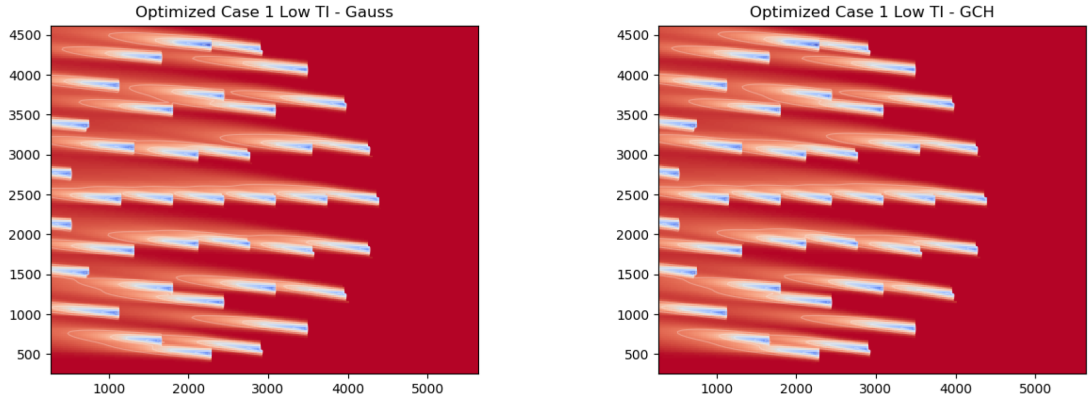


**Figure 13.** Flow fields of the optimized Gaussian model (left) and the optimized GCH model (right) for Case 1 where the wind direction is at 95°.

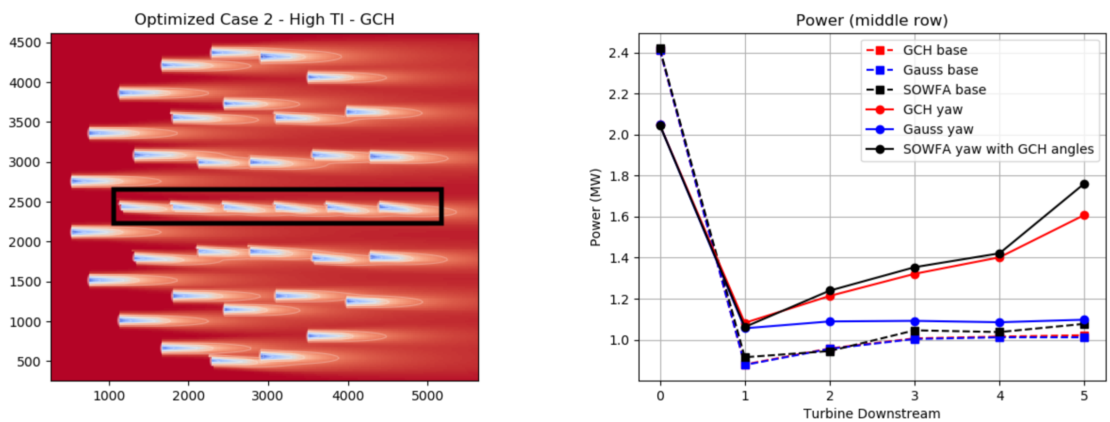


**Figure 14.** Flow ~~fields~~ field of the optimized ~~Gaussian~~ GCH model (left) ~~and the optimized GCH model (right)~~ is shown for Case 2 where the wind direction is at 270° with turbulence intensity of 10%. The power of the centerline of turbines, indicated by the black box, is shown on the right for the Gaussian model, GCH, and SOWFA.

| Case | SOWFA Total Power Gain | Gauss Total Power Gain | GCH Total Power Gain |
|---|---|---|---|
| | | Low Turbulence | |
| Case 1 - ~~Gauss-optimized~~ Gauss optimized angles | 7.6% | ~~5.0~~5.9% | ~~7.7~~7.6% |
| Case 1 - ~~GCH-optimized~~ GCH optimized angles | **8.0**% | ~~4.5~~5.4% | ~~8.5~~7.9% |
| Case 2 - ~~Gauss-optimized~~ Gauss optimized angles | 3.8% | ~~2.3~~2.6% | ~~4.7~~5.3% |
| Case 2 - ~~GCH-optimized~~ GCH optimized angles | **~~4.3~~4.0**% | ~~1.5~~2.1% | 5.5% |
| | | High Turbulence | |
| Case 1 - ~~Gauss-optimized~~ Gauss optimized angles | ~~4.4~~4.1% | ~~2.7~~3.3% | ~~5.9~~4.4% |
| Case 1 - ~~GCH-optimized~~ GCH optimized angles | **4.5**% | ~~2.2~~3.0% | ~~6.4~~4.5% |
| Case 2 - ~~Gauss-optimized~~ Gauss optimized angles | 2.3% | ~~0.8~~1.2% | ~~3.1~~3.0% |
| Case 2 - ~~GCH-optimized~~ GCH optimized angles | **3.1**% | ~~0.3~~0.7% | ~~3.6~~3.1% |

**Table 2.** Wind farm results for ~~low-~~ low and ~~high-turbulence~~ high turbulence conditions for SOWFA, the Gaussian model, and the GCH model.

Optimizations were performed with the Gaussian model and the GCH model for ~~low-~~ low (6%) and ~~high-~~ high (10%) turbulence conditions. Flow fields are shown in Fig. 13 for the Gaussian model (left) and the GCH model (right) for Case 1 of 95° ~~,~~ and Fig. 14 shows the ~~Gaussian~~ GCH (left) ~~and GCH (right)~~ model for Case 2 of 270° ~~(bottom).~~ under low turbulence conditions and the power of the center line of turbines indicated by the black box in the left figure for SOWFA, the GCH model, and the Gaussian model under baseline and optimized yaw angles. The optimized yaw angles used in Fig. 14 are the optimized yaw angles for the GCH model.

The results of the optimization are shown in Table 2. The optimized yaw angles from the Gaussian model and the GCH model were tested in SOWFA. As with the ~~five-turbine~~ five turbine case, the yaw angles produced in the optimization with the GCH model had the largest gain in SOWFA. In addition, the gains computed by the GCH model are closer to the gains in the SOWFA results than the Gaussian model ~~,~~ indicating that the GCH model is better able to capture the secondary effects of the large-scale flow structures generated by misaligned turbines.

Lastly, a full optimization over a wind rose was run for the wind farm in ~~low- and high-turbulence~~ low and high turbulence conditions. The wind rose is shown in Fig. 15 to compute annual energy production (AEP). The Gaussian model and the GCH model were optimized for wake steering over this wind rose ~~,~~ and the AEP gains are reported in Table 3. The Gaussian model predictions of AEP gains are less than half of the gains predicted by the GCH model under both ~~low- and high-turbulence~~ low and high turbulence conditions. This is a promising result for understanding the full potential of wake steering in large wind farms. By taking advantage of these large-scale flow structures, there is more potential for increasing the power production in a wind farm and it is more representative of what is happening within the wind farm as has been shown throughout this paper.

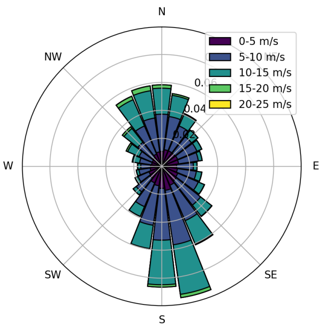


**Figure 15.** Wind rose used to compute the AEP gains from wake steering.

| Annual Energy Production Results | | |
|---|---|---|
| Model | Low Turbulence, TI = 6.5% | High Turbulence, TI = 9% |
| Gauss | 1.3% | 0.7% |
| GCH | ~~2.8~~2.2% | ~~2.1~~1.6% |

**Table 3.** Wind farm AEP results for low and high TI.

## 6 Conclusion

This paper introduces an analytical model that better captures the secondary effects of wake steering in a large wind farm. These secondary effects include yaw-added wake recovery ~~that significantly boost~~ as well as secondary wake steering that significantly boosts the impact of wake steering. The results of this model were compared with LES for ~~two-, three-, and five-turbine arrays~~ three, and five turbine arrays as well as a 38-turbine wind farm. The model compared well with results from ~~the~~ LES and outperformed the Gaussian model in most cases. Furthermore, this paper demonstrated the possible gains in a large wind farm when considering these large-scale flow structures. Controllers can be developed in the future to manipulate these flow structures to significantly improve the performance of a wind farm.

*Acknowledgements.* This work was authored [in part] by the National Renewable Energy Laboratory, operated by Alliance for Sustainable Energy, LLC, for the U.S. Department of Energy (DOE) under Contract No. DE-AC36-08GO28308. Funding provided by the U.S. Department of Energy Office of Energy Efficiency and Renewable Energy Wind Energy Technologies Office. The views expressed in the article do not necessarily represent the views of the DOE or the U.S. Government. The U.S. Government retains and the publisher, by accepting the article for publication, acknowledges that the U.S. Government retains a nonexclusive, paid-up, irrevocable, worldwide license to publish or reproduce the published form of this work, or allow others to do so, for U.S. Government purposes.

## References

Abkar, M. and Porté-Agel, F.: The effect of atmospheric stability on wind-turbine wakes: A large-eddy simulation studys, in: The Science of Making Torque from Wind, Lyngby, Denmark, 2014.

Abkar, M. and Port-Agel, F.: Influence of atmospheric stability on wind-turbine wakes: A large-eddy simulation study, Physics of Fluids, 27, doi:10.1063/1.4913695, 2015.

Annoni, J., Fleming, P., Scholbrock, A., Roadman, J., Dana, S., Adcock, C., Porte-Agel, F., Raach, S., Haizmann, F., and Schlipf, D.: Analysis of Control-Oriented Wake Modeling Tools Using Lidar Field Results, Wind Energy Science Discussions, 2018, 1–17, doi:10.5194/wes-2018-6, https://www.wind-energ-sci-discuss.net/wes-2018-6/, 2018.

Annoni, J., Dall'Anese, E., Hong, M., and Bay, C. J.: Efficient Distributed Optimization of Wind Farms Using Proximal Primal-Dual Algorithms, in: 2019 American Control Conference (ACC), pp. 4173–4178, IEEE, 2019.

Bastankhah, M. and Porté-Agel, F.: Wind farm power optimization via yaw angle control: A wind tunnel study, Journal of Renewable and Sustainable Energy, 11, 023 301, 2019.

Bastankhah, M. and Porté-Agel, F.: A new analytical model for wind-turbine wakes, Renewable Energy, 70, 116–123, 2014.

Bastankhah, M. and Porté-Agel, F.: Experimental and theoretical study of wind turbine wakes in yawed conditions, Journal of Fluid Mechanics, 806, 506–541, 2016.

Bay, C. J., Annoni, J., Martínez-Tossas, L. A., Pao, L. Y., and Johnson, K. E.: Flow Control Leveraging Downwind Rotors for Improved Wind Power Plant Operation, in: 2019 American Control Conference (ACC), pp. 2843–2848, IEEE, 2019.

Churchfield, M. J., Lundquist, J. K., Quon, E., Lee, S., and Clifton, A.: Large-Eddy Simulations of Wind Turbine Wakes Subject to Different Atmospheric Stabilities, in: American Geophysical Union Fall Meeting, 2014.

Ciri, U., Rotea, M. A., and Leonardi, S.: Effect of the turbine scale on yaw control, Wind Energy, 21, 1395–1405, 2018.

Crespo, A., Hernández, J., and Frandsen, S.: Survey of modelling methods for wind turbine wakes and wind farms, Wind Energy, 2, 1–24, 1999.

Damiani, R., Dana, S., Annoni, J., Fleming, P., Roadman, J., van Dam, J., and Dykes, K.: Assessment of Wind Turbine Component Loads Under Yaw-Offset Conditions, Wind Energy Science Discussions, 2017, 1–25, doi:10.5194/wes-2017-38, https://www.wind-energ-sci-discuss.net/wes-2017-38/, 2017.

Fleming, P., Aho, J., Gebraad, P., Pao, L., and Zhang, Y.: CFD Simulation Study of Active Power Control in Wind Plants, in: American Control Conference, 2016.

Fleming, P., Annoni, J., Churchfield, M., Martinez-Tossas, L. A., Gruchalla, K., Lawson, M., and Moriarty, P.: A simulation study demonstrating the importance of large-scale trailing vortices in wake steering, Wind Energy Science, 3, 243–255, doi:10.5194/wes-3-243-2018, https://www.wind-energ-sci.net/3/243/2018/, 2018a.

Fleming, P., Annoni, J., Martínez-Tossas, L. A., Raach, S., Gruchalla, K., Andrew Scholbrock, Churchfield, M., and Roadman, J.: Investigation into the shape of a wake of a yawed full-scale turbine, Journal of Physics: Conference Series, 1037, 032 010, http://stacks.iop.org/1742-6596/1037/i=3/a=032010, 2018b.

Fleming, P., King, J., Dykes, K., Simley, E., Roadman, J., Scholbrock, A., Murphy, P., Lundquist, J. K., Moriarty, P., Fleming, K., van Dam, J., Bay, C., Mudafort, R., Lopez, H., Skopek, J., Scott, M., Ryan, B., Guernsey, C., and Brake, D.: Initial results from a field campaign of wake steering applied at a commercial wind farm – Part 1, Wind Energy Science, 4, 273–285, doi:10.5194/wes-4-273-2019, https://www.wind-energ-sci.net/4/273/2019/, 2019a.

Fleming, P., King, J., Simley, E., Roadman, J., Scholbrock, A., Murphy, P., Lundquist, J. K., Moriarty, P., Fleming, K., van Dam, J., Bay, C., Mudafort, R., Lopez, H., Skopek, J., Scott, M., Ryan, B., Guernsey, C., and Brake, D.: Continued Results from a Field Campaign of Wake Steering Applied at a Commercial Wind Farm: Part 2, Submitted to Wind Energy Science, 2019b.

Gebraad, P., Teeuwisse, F., Wingerden, J., Fleming, P. A., Ruben, S., Marden, J., and Pao, L.: Wind plant power optimization through yaw control using a parametric model for wake effects—a CFD simulation study, Wind Energy, 19, 95–114, 2016.

Gebraad, P., Thomas, J. J., Ning, A., Fleming, P., and Dykes, K.: Maximization of the annual energy production of wind power plants by optimization of layout and yaw-based wake control, Wind Energy, 20, 97–107, 2017.

Howland, M. F., Bossuyt, J., Martínez-Tossas, L. A., Meyers, J., and Meneveau, C.: Wake structure in actuator disk models of wind turbines in yaw under uniform inflow conditions, Journal of Renewable and Sustainable Energy, 8, 043 301, doi:10.1063/1.4955091, 2016.

Jensen, N. O.: A note on wind generator interaction, Tech. Rep. Risø-M-2411, Risø National Laboratory, 1984.

Jiménez, Á., Crespo, A., and Migoya, E.: Application of a LES technique to characterize the wake deflection of a wind turbine in yaw, Wind energy, 13, 559–572, 2010.

Katić, I., Højstrup, J., and Jensen, N. O.: A simple model for cluster efficiency, in: EWEA Conference and Exhibition, pp. 407–410, Rome, Italy, 1986.

Martínez-Tossas, L. A., Annoni, J., Fleming, P. A., and Churchfield, M. J.: The aerodynamics of the curled wake: a simplified model in view of flow control, Wind Energy Science (Online), 4, 2019.

Martínez-Tossas, L. A., Churchfield, M. J., and Leonardi, S.: Large eddy simulations of the flow past wind turbines: actuator line and disk modeling, Wind Energy, 18, 1047–1060, 2015.

Medici, D. and Alfredsson, P.: Measurements on a wind turbine wake: 3D effects and bluff body vortex shedding, Wind Energy, 9, 219–236, 2006.

Niayifar, A. and Porté-Agel, F.: A new analytical model for wind farm power prediction, in: Journal of Physics: Conference Series, vol. 625, p. 012039, IOP Publishing, 2015.

NREL: FLORIS. Version 1.1.4, https://github.com/NREL/floris, 2019.

Pope, S. B.: Turbulent flows, 2001.

Schottler, J., Hölling, A., Peinke, J., and Hölling, M.: Wind tunnel tests on controllable model wind turbines in yaw, in: 34th Wind Energy Symposium, p. 1523, 2016.

Shapiro, C. R., Gayme, D. F., and Meneveau, C.: Modelling yawed wind turbine wakes: a lifting line approach, Journal of Fluid Mechanics, 841, 2018.

Simley, E., Fleming, P., and King, J.: Design and Analysis of a Wake Steering Controller with Wind Direction Variability, Wind Energy Science Discussions, 2019, 1–26, doi:10.5194/wes-2019-35, https://www.wind-energ-sci-discuss.net/wes-2019-35/, 2019.

Stanley, A. P. J. and Ning, A.: Massive Simplification of the Wind Farm Layout Optimization Problem, Wind Energy Science Discussions, 2019, 1–20, doi:10.5194/wes-2019-37, https://www.wind-energ-sci-discuss.net/wes-2019-37/, 2019.

Stull, R. B.: An introduction to boundary layer meteorology, vol. 13, Springer Science & Business Media, 2012.

Thomas, J. J., Annoni, J., Fleming, P. A., and Ning, A.: Comparison of Wind Farm Layout Optimization Results Using a Simple Wake Model and Gradient-Based Optimization to Large Eddy Simulations, in: AIAA Scitech 2019 Forum, p. 0538, 2019.

Vollmer, L., Steinfeld, G., Heinemann, D., and Kühn, M.: Estimating the wake deflection downstream of a wind turbine in different atmospheric stabilities: an LES study, Wind Energy Science, 1, 129–141, 2016.

Wagenaar, J., Machielse, L., and Schepers, J.: Controlling wind in ECN's scaled wind farm, Proc. Europe Premier Wind Energy Event, pp. 685–694, 2012.